nature physics

Article

https://doi.org/10.1038/s41567-022-01899-z

Anyonic interference and braiding phase in a Mach-Zehnder interferometer

Received: 24 March 2022

Accepted: 25 November 2022

Published online: 23 January 2023

Check for updates

Hemanta Kumar Kundu [1], Sourav Biswas [1], Nissim Ofek[2], Vladimir Umansky[1] & Moty Heiblum [1]

Fractional quantum Hall states have long been predicted to be a testing ground of fractional—anyonic—exchange statistics. These topological states, which can have either an Abelian or non-Abelian character, harbour quasiparticles with fractional charges. The charge of the quasiparticles can be measured by shot noise measurements, whereas their quantum statistics can be revealed by appropriate interference experiments. The multipath Fabry–Pérot electronic interferometer is easier to fabricate, but it is often plagued by Coulomb interactions, area breathing with the magnetic field and fluctuating charges. Yet, recent experiments with an adequately screened Fabry–Pérot interferometer allowed the observation of anyonic interference at a bulk filling factor of $\nu = 1/3$. Here we demonstrate the interference and braiding of anyons in an interaction-free two-path Mach–Zehnder interferometer tuned to bulk filling of $\nu = 2/5$ with an outermost $\nu = 1/3$ edge mode. Interference with this mode reveals a phase dependence that corresponds to the predicted anyonic braiding. This proves that a Mach–Zehnder interferometer is a powerful tool that probes the quantum statistics of complex anyonic states.

Quantum Hall effect states were the earliest protagonists of topological phases of matter. Although the bulk is insulating, the current is carried by gapless chiral edge modes with a universal edge conductance of $\boldsymbol{\nu}e^2/h$, where e is the electron charge, h is the Planck constant and $\boldsymbol{\nu}$ is the filling factor (integer or fraction)[1–3]. In the fractional regime, that is, the fractional quantum Hall effect, the excitations are quasiparticles, each carrying a fractional charge with an attached flux[4–10]. The quasiparticles are neither bosons nor fermions—they are classified as anyons[11,12]. On exchanging two identical quasiparticles, the phase of their joint wavefunction changes by a fraction of π, whereas it is π for fermions and 2π for bosons[8,13,14].

Ideally, observing the statistics of the quasiparticles can be accomplished by interfering edge modes around localized quasiparticles in the bulk. The two best-studied electronic interferometers are the Fabry–Pérot interferometer (FPI)[4,15–24] and Mach–Zehnder interferometer (MZI)[25–33]. The FPI (a large version of a quantum dot (Fig. 1b)) possesses a finite charging energy for the addition of quasiparticles[23,34,35], which tends to blur the interference. However, recent experiments with screened FPIs enabled the observation of anyonic Aharonov–Bohm (AB) interference[21,22]. The MZI is free of charging effects since one of its drains is located in its interior, thus adding or removing particles at will (Fig. 1a); however, thus far, interference was only observed in the integer quantum Hall regime[25–27,33]. The apparent lack of anyonic interference was attributed to the relatively large interferometer size, poor quality of interior drain contact and presence of non-topological neutral modes[36–42].

Here we describe the observation of high-visibility interference of the outer $\boldsymbol{\nu} = 1/3$ edge mode in a bulk filling factor of $\boldsymbol{\nu} = 2/5$, employing an optimized MZI. As detailed below, the anyonic MZI is unique because bare AB interference is naturally dressed by an added anyonic braiding phase. The dressing results from the natural inclusion (into the AB loop) of the already interfered quasiparticles, leading to an added braiding phase to the bare AB phase (Fig. 1a). Our measurements support the theoretical prediction that Laughlin's quasiparticles are expected to exhibit an interference periodicity of a single flux quantum[30,31,43–47]. Below, we describe the interferometer structure, experimental results

[1]Braun Center for Submicron Research, Department of Condensed Matter Physics, Weizmann Institute of Science, Rehovot, Israel. [2]Quantum Machines, Tel Aviv, Israel. e-mail: moty.heiblum@weizmann.ac.il

https://doi.org/10.1038/s41567-022-01899-z

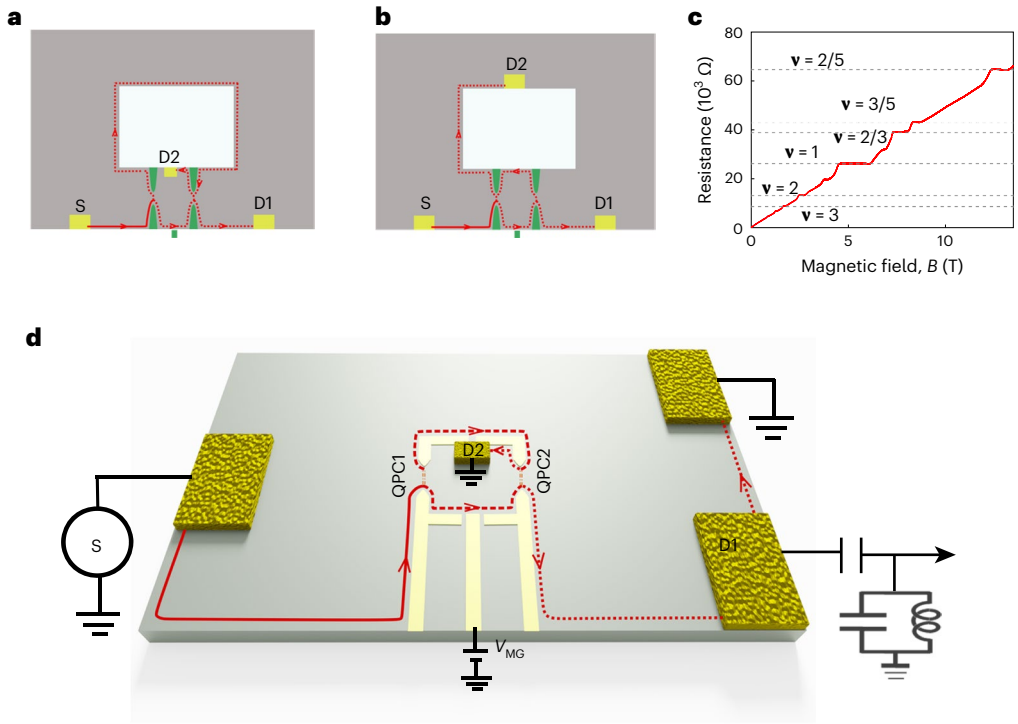

Fig. 1 | Device structure and conductance quantization. a,**b**, Schematic of MZI (**a**) and FPI (**b**). The difference in the position of drain D2 makes the interferometers fundamentally different, especially in the fractional regime. **c**, Two-probe Hall resistance as a function of magnetic field. The distinct quantization of quantum Hall plateaus is observed. **d**, Schematic of our measurement setup. A chiral edge mode injected by source S impinges on the first beamsplitter (QPC1) and splits into two paths guided by 'gate-defined' paths, which later recombine and interfere at QPC2. This results in two outputs measured by drains D1 and D2. When the phase between the two paths varies, the signals oscillate out of phase in D1 relative to D2. The area enclosed by the dashed lines determines the AB flux.

and a brief sketch of the theoretical arguments, followed by a simplified toy model that provides a better 'feel' of the anyonic interference, agreeing with the experimental results.

The MZI is formed by two closely placed quantum point contacts (QPCs), acting as partitioning beamsplitters and two ohmic contacts serving as drains: D2, a small, grounded contact on the inner periphery; D1, a contact located downstream from the MZI (Fig. 1a,d). The impinging edge mode partitions in QPC1, with the resultant two trajectories rejoin in QPC2, thus enclosing a magnetic flux. Note that there is a π-phase difference between the transmission (t_i) and reflection (r_i) amplitudes in each QPC. The transmission probabilities in the integer regime are

$$T_{D1} = |t_1t_2 + r_1r_2e^{i2\pi\phi/\phi_0}|^2 = |t_1t_2|^2 + |r_1r_2|^2 + 2|t_1t_2r_1r_2|\cos(2\pi\phi/\phi_0), \quad (1a)$$

$$T_{D2} = |t_1r_2 + r_1t_2e^{i2\pi\phi/\phi_0}|^2 = |t_1r_2|^2 + |r_1t_2|^2 - 2|t_1t_2r_1r_2|\cos\left(\frac{2\pi\phi}{\phi_0}\right), \quad (1b)$$

where ϕ/ϕ_0 is the number of flux quanta threading the area enclosed by the two trajectories, and $T_{D1} + T_{D2} = 1$. A modulation gate (MG) tunes the threaded flux by changing the enclosed area. The visibility of electrons is defined as $v_e = \frac{T_{max}-T_{min}}{T_{max}+T_{min}}$, where T_{max} and T_{min} are the maximum and minimum transmission at each drain, respectively.

We studied two different-sized MZIs. One with an effective area of 3.67 μm^2 and a larger one with an area of 13.50 μm^2 (Supplementary Fig. 1), with single path lengths of 1.9 and 5.1 μm, respectively. The MZIs were fabricated in a high-mobility two-dimensional (2D) electron gas embedded in a GaAs/AlGaAs heterostructure. We tested two different molecular-beam-epitaxy-grown 2D electron gases with electron density of 0.92 and 1.22 × 10^{11} cm^{-2} and 4.2 K dark mobility of 4.1 and 3.6 × 10^6 cm^2 V^{-1} s^{-1}, respectively, at electronic temperatures in the range of 10–15 mK. We devoted particular effort to fabricate a low-resistance inner drain D2 (Supplementary Section 1). Conductance and shot noise were measured at 900 kHz, with an appropriate bandwidth in each case. A homemade pre-amplifier, cooled to 1.5 K, cascaded by a room-temperature amplifier, provided a total gain of ≈5,000. The measurement results are summarized in Table 1.

We first studied the smaller MZI with the magnetic field tuned to bulk fillings of **ν** = 3 and **ν** = 2. The 2D pyjama plot (conductance in the V_{MG}–B plane) of the interfering outermost edge mode (closest to the edge and furthermost to the bulk) of **ν** = 2 is shown in Fig. 2a. The periodicity is of a flux quantum, $\phi_0 = h/e$, and the plot is characteristic of AB interference with a constant area[25] (Fig. 2a,b, Table 1, Supplementary Section 2 and Supplementary Fig. 2). In both fillings of **ν** = 3 and **ν** = 2, the innermost edge mode (closest to the bulk) did not exhibit interference, probably due to dephasing caused by the inner drain (due to a finite bulk resistance). The general behaviour of the larger MZI was similar to that of the smaller MZI but with lower visibility (Table 1 and Supplementary Section 8).

Assuming a constant MG capacitance C, it depletes a charge $\Delta q = C\Delta V_{MG} = n_e e\Delta A$, where n_e is the density and ΔA is the depleted area. Consequently, the AB phase changes by $\Delta\varphi = 2\pi\frac{B\Delta A}{\phi_0}$, with flux ratio of $\frac{\Delta\phi_2}{\Delta\phi_1} = \frac{B_2\Delta V_{MG2}}{B_1\Delta V_{MG1}}$ (Supplementary Section 3). In particular, the expelled charge per period (a single flux quantum) was $\Delta q(\nu = 2) = 2e$ and $\Delta q(\nu = 3) = 3e$ (Table 1).

The highest visibility, $v_e \approx 91\%$, remained constant for all the values of $T_{MZI\text{-}D1} \leq 0.5$ (to be distinguished from the maximum interference

https://doi.org/10.1038/s41567-022-01899-z

Table 1 | Details of interference at integer and fractional quantum Hall regimes

Device size (2D density)	ν	B (T)	ΔB (Gauss)	$\Delta\phi$ (ϕ_0)	ΔV_{MG} (mV)	$\Delta\|q\|$ (e)	$\frac{\Delta\phi_2}{\Delta\phi_1} = \frac{B_2\Delta V_{MG2}}{B_1\Delta V_{MG1}}$	Visibility (%)
3.67 μm² (high density)	2	2.5	10.8	1	22.2	2	1	90.7
	3	1.675	10.96	1.01	32.9	2.96	1.01	62.4
	2/5	12.65	10.59	0.98	4.2	0.38	1.04	22.0
13.50 μm² (low density)	2	1.85	3.02	1	9.8	2	1	67.6
	3	1.245	3.02	1.0	14.7	3.0	0.99	13.9
	2/5	9.05	2.91	0.96	1.8	0.37	1.10	8.3

The normalization is with respect to the interference of the outer edge in **ν**=2 with an electron.

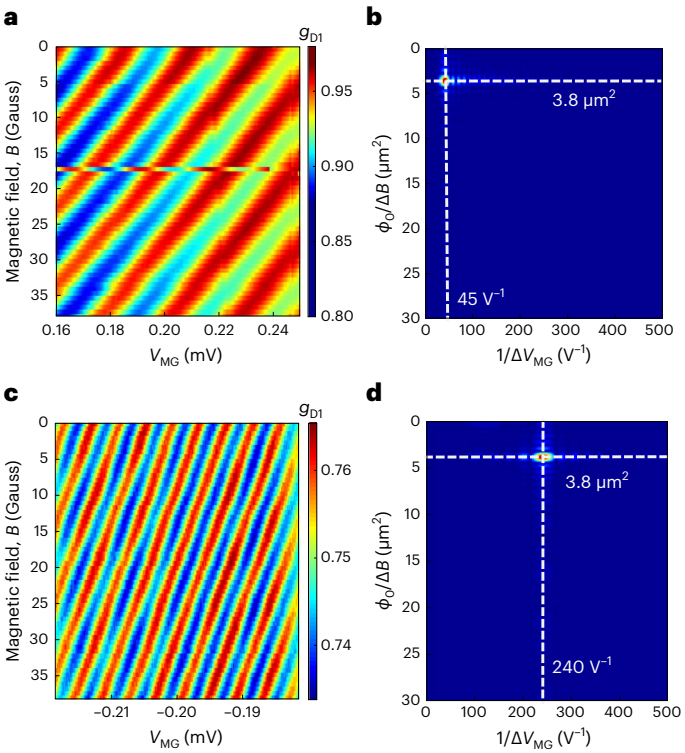

Fig. 2 | Integer and fractional AB interference patterns. a,**c**, 'Pyjama plots': conductance oscillation (g_{D1}) with interfering outer edge mode in the V_{MG}–B plane. Interference of the outer edge mode in bulk filling of **ν** = 2 (B = 2.5 T) (**a**). Interference of the outer edge mode (**ν** = 1/3) in bulk filling of **ν** = 2/5 (B = 12.65 T). The equiphase lines are typical of AB interference. In both states, the field periodicity is of a single flux quantum. **b**,**d**, 2D Fourier transforms of the pyjama plots showing a single peak, excluding Coulomb effects. The two periodicities in V_{MG}, namely, 22.2 mV in **ν** = 2 and 4.2 mV in **ν** = 2/5, are proportional to 1/B.

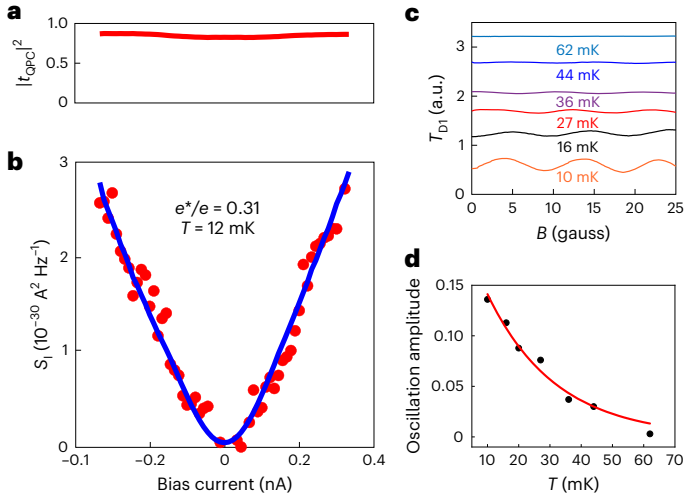

Fig. 3 | Charge determination via shot noise measurements and temperature-dependent visibility. a, Nonlinear differential transmission of the partitioned 1/3 outer edge mode by a QPC (at bulk filling of **ν** = 2/5), where $|t_{QPC}|^2 \approx 0.82$. **b**, Current-dependent spectral density of the shot noise (red discrete data points). The fit (blue line) agrees with charge $e^* = 0.31e$ at electronic temperature of 12 mK. **c**, Temperature dependence of the B-dependent interfering traces of the 1/3 mode. **d**, Exponential fit of the temperature-dependent interfering oscillations leads to a characteristic temperature of 23 mK.

amplitude at the half transmission of MZI, namely, $T_{MZI\text{-}D1} = 0.5$). The visibility gradually diminished with an increase in the magnetic field, ultimately disappearing altogether at **ν** = 1 (Supplementary Section 4). The previously observed dependence could result from the absence of an inner (screening) mode and/or a spontaneous edge reconstruction that may have led to short-range non-topological neutral modes[32,33,36,37].

Bulk filling of **ν** = 2/5 supports two downstream edge modes with conductance of $e^2/15h$ (inner edge and closest to the bulk) and $e^2/3h$ (outer edge and closest to the edge) (Supplementary Section 5 and Supplementary Fig. 4). The inner edge is reflected first by the QPC, as we pinch it to partition at the outer edge. The two QPCs were tuned to partition the outer **ν** = 1/3 edge mode and fully backscatter the inner **ν** = 1/15 mode. Care was taken to assure (via shot noise measurements) the partitioned quasiparticles charge is $e/3$ (Fig. 3a,b). Partitioning the inner edge mode leads to a quasiparticle charge of $e/5$ (Supplementary Section 6).

The observed periodicity in B was of a single flux quantum (Fig. 2c,d and Table 1). At the same time, the periodicity in V_{MG} corresponded to a depleted charge of $\Delta q \cong 0.4e$—corresponding to an expelled single flux quantum (Table 1 and Supplementary Section 3). Similar periodicities were found in the larger MZI (Table 1 and Supplementary Section 8). The interference diminished exponentially with increasing temperature, with a characteristic temperature of 23 mK (Fig. 3c,d). Comparing the visibilities in the two MZIs, we estimate a typical dephasing length of 10.5 μm for electrons and 3.3 μm for quasiparticles.

An intermediate summary: the present data of interfering $e/3$ quasiparticles, expected by theory[18,30,31,43–47], proves that an anyonic MZI is fairly different from an anyonic FPI. In the FPI, the B-dependent flux periodicity is $3\phi_0$, whereas the V_{MG} repels the charge $\Delta q = e$ per period, corresponding to three $e/3$ quasiparticles depleted from the interfering Landau level[21]. Comparison of FPI and MZI: FPI, flux periodicity of quasiparticles charge e/m is $m\phi_0$, and gate-depleted charge

https://doi.org/10.1038/s41567-022-01899-z

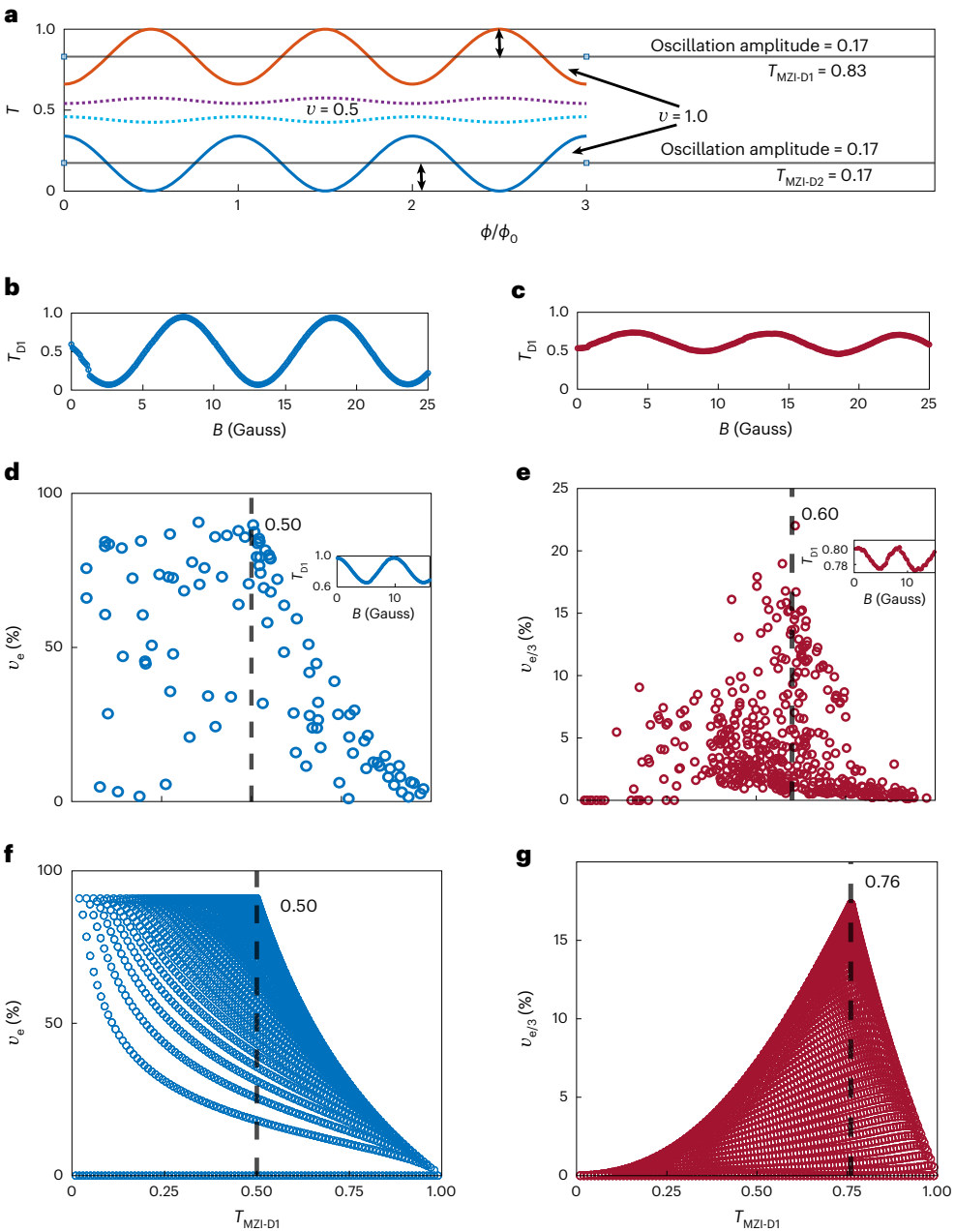

Fig. 4 | Visibility in the integer and fractional regimes. a, Calculated anyonic interference patterns in the two drains, D1 and D2 (equations (1a) and (1b)). The solid orange and blue lines represent the maximum interference amplitude (at $|t_i|^2 = 0.5$), which is expected at D1 and D2 for $\upsilon_e = 1$. Although the oscillation amplitudes at D1 and D2 are the same (but out of phase), the average transmissions are very different ($T_{MZI-D1} \approx 5 \times T_{MZI-D2}$), indicating visibility at D1 (20%, $T_{MZI} \approx 0.83$) to be almost five times smaller than at D2 (100%, $T_{MZI} \approx 0.17$). The visibility drops off rapidly with a diminishing υ_e. This is shown by dotted oscillations (purple and cyan) for $\upsilon_e = 0.5$. **b**, Traces of the measured interference oscillation of the interfering outer $\mathbf{v} = 1$ mode at bulk filling of $\mathbf{v} = 2$ ($B = 2.5$ T). **c**, A similar plot of the measured interfering outer $\mathbf{v} = 1/3$ mode at bulk filling of $\mathbf{v} = 2/5$ ($B = 12.65$ T). **d**,**e**, Measured visibilities in the integer (**d**) and fractional (**e**) regimes as a function of average transmission T_{MZI-D1}. Each dot represents a different combination of the QPCs' transmissions ($|t_1|^2$ and $|t_2|^2$). In the fractional regime, the QPCs' individual transmissions were kept relatively high around the peak value of visibility to assure a Fano factor of 1/3 at each QPC. The inset shows the representative interference traces at a very weak backscattering limit. Strong backscattering, where bunching of quasiparticles takes place, is avoided. Interestingly, interference at strong backscattering is suppressed. **f**,**g**, Calculated visibility at D1 for integer (**f**) and fractional (**g**) regimes. The points in the line shape are for single $|t_1|^2$, whereas $|t_2|^2$ is varied for all the possible values in steps. The different lines correspond to multiple values of $|t_1|^2$, covering both QPC limits. The striking difference between these two visibilities emanates from the different braiding phases of the electrons and fractional charges (Supplementary Section 7). The measured υ_e dependence on T_{MZI-D1} is in accordance with $\eta = 0.91$ (**d**,**f**). Assuming the same η, the $\upsilon_{e/3}$ profile as a function of T_{MZI-D1} matches fairly well the experimental one. The measured visibility peak is $\upsilon_{e/3} \approx 22.0\%$ at $T_{MZI-D1} \approx 0.60$, whereas the expected peak is $\upsilon_{e/3} \approx 15.6\%$ at $T_{MZI-D1} \approx 0.76$.

of $\Delta q = m\mathbf{v}e$ per period; MZI, flux periodicity is ϕ_0, and gate-depleted charge $\Delta q = \mathbf{v}e$ per period.

The predicted and observed flux periodicity in the anyonic MZI is ϕ_0—manifesting the dressed AB interference—which combines the bare AB phase with anyonic braiding[30,31,43–47]. Anyonic braiding strongly affects the visibility of the MZI. For electrons, the average transmission is $T_{MZI-D1} = |t_1 t_2|^2 + |r_1 r_2|^2$ and the visibility is $\upsilon_e = \frac{2\eta|t_1 t_2 r_1 r_2|}{T_{MZI-D1}}$, where η is a

dephasing factor. The visibility increases smoothly from zero at $T_{\mathrm{MZI\text{-}D1}} = 1.0$ ($T_{\mathrm{MZI\text{-}D2}} = 0$) with a maximum at $T_{\mathrm{MZI\text{-}D1}} = T_{\mathrm{MZI\text{-}D2}} = 0.5$. For $T_{\mathrm{MZI\text{-}D1}} < 0.5$, the maximum visibility remains constant (Fig. 4f). However, in the $\boldsymbol{\nu} = 1/3$ regime, the observed visibility in outer drain D1, $\upsilon_{e/3}$, is expected to peak sharply at $T_{\mathrm{MZI\text{-}D1}} > 0.5$ ($T_{\mathrm{MZI\text{-}D2}} < 0.5$) and fall on each side of the peak. The expected interference visibility is markedly different in the two drains (Fig. 4g).

Interference periodicity in the MZI, which is ϕ_0 in the integer and fractional regimes, has already been theoretically predicted[4,30,31,43–46]. The latter resulted from an added braiding phase to the bare anyonic AB phase[4,30,31,43–46]. Although this is not the place to discuss theories in any detail, we highlight the main difference between MZI and FPI and accompany it with an unrealistic toy model that nevertheless agrees with the interference periodicity and unexpected visibility, as well as gives some intuitive insight into the physics. In the MZI, the incoming edge mode splits into two trajectories that interfere with the resultant two output edge modes—one absorbed by the outer drain (D1) and the other absorbed by the internal drain (D2). In the FPI, the incoming edge mode also splits into two trajectories—one reflected and one splits further and interferes with itself—with both outputs absorbed by external drains. The critical difference between the two interferometers is the reabsorption of an interfered trajectory by the inner drain (D2) of the MZI[4]. The presence of added quasiparticles in the inner volume of the MZI leads to an added statistical phase and thus modifies the bare AB phase. Theoretically, this unique inner reabsorption affects the anyonic tunnelling (partitioning) operators of the QPCs[2], expressed by the so-called Klein factors[30,43,46,48,49], which obey fractional statistics. The commutation relations of the Klein factors[30,31,43–46] dictate a flux periodicity of ϕ_0 (ref. [30]).

Based on these theoretical arguments, we provide below (Supplementary Section 7) an illuminating toy model that captures the essence of the theories (dressed AB phase). This unrealistic model relies on the unique absorption of quasiparticles by drain D2. Namely, D2 can absorb only electrons (each with its three flux quanta), thus leading to mode-3 cycles (of entering $e/3$ quasiparticles), which results in ϕ_0 periodicity.

When the AB phase directs a quasiparticle to drain D2, it is screened by holes in the drain, whereas its attached flux remains uncompensated (effectively occupying the area of a flux quantum). For each of the next two quasiparticles, a braiding phase of $\frac{2\pi}{3}$ is added to the bare AB anyonic phase. Hence, the evolving dressed AB phase for the nth quasiparticle is

$$\varphi_{\mathrm{AB}} = 2\pi\left(\frac{\phi}{3\phi_0} + \frac{n}{3}\right) \tag{2}$$

where the $(n+1)$th interfering quasiparticle enters the MZI and the nth flux quantum gets stuck at drain D2. After three consecutive quasiparticles reach the drain, they are absorbed as an electronic charge with three flux quanta attached, and the phase will return to its initial value (repeating in modulo 3). This counterintuitive mechanism has an extraordinary consequence on the visibility and periodicity of the interference pattern (Supplementary Section 7); yet, it explains our observed experimental data.

The time required for the $(n+1)$th quasiparticle to arrive at D2 is $t_n = 1/p_n$, where p_n is its probability of arriving at D2 per unit time. This probability is $p_n = T_{\mathrm{I}}(1 + \upsilon_{\mathrm{e}} \cos 2\pi(\frac{\phi}{3\phi_0} + \frac{n}{3}))$, where $T_{\mathrm{I}} = |t_1 r_2|^2 + |r_1 t_2|^2$, the flux-independent probability determined by transmission $|t_i|^2$ of each QPC[30,50]. The expected transmission to D2 is

$$\begin{aligned} T_{\mathrm{D2}} &\equiv 3\left[\sum_{n=0}^{2}\frac{1}{p_n}\right]^{-1} = 3T_{\mathrm{I}}\sum_{n=0}^{2}\left[\frac{1}{1+\upsilon_{\mathrm{e}}\cos\left(\frac{2\pi\phi}{3\phi_0}+\frac{2\pi n}{3}\right)}\right]^{-1} \\ &= T_{\mathrm{I}}\frac{4-3\upsilon_{\mathrm{e}}^2}{4-\upsilon_{\mathrm{e}}^2}\left[1+\frac{\upsilon_{\mathrm{e}}^3}{4-3\upsilon_{\mathrm{e}}^2}\cos\left(\frac{2\pi\phi}{\phi_0}\right)\right] \end{aligned} \tag{3}$$

Due to current conservation, the transmission to downstream drain D1 is

$$T_{\mathrm{D1}} = 1 - T_{\mathrm{D2}} = \left(1 - T_{\mathrm{I}}\frac{4-3\upsilon_{\mathrm{e}}^2}{4-\upsilon_{\mathrm{e}}^2}\right) - T_{\mathrm{I}}\frac{\upsilon_{\mathrm{e}}^3}{4-\upsilon_{\mathrm{e}}^2}\cos\left(\frac{2\pi\phi}{\phi_0}\right) \tag{4}$$

A few essential features of anyonic interference are apparent: (1) flux periodicity is ϕ_0; (2) the two drains are not equivalent; (3) the oscillation amplitude is substantially lower than for electrons (for ideally similar decoherence rates). The expected visibility at D1 is

$$\upsilon_{e/3} = T_{\mathrm{I}}\upsilon_{\mathrm{e}}^3/[(4-\upsilon_{\mathrm{e}}^2) - T_{\mathrm{I}}(4-3\upsilon_{\mathrm{e}}^2)] \tag{5}$$

reaching a maximum, depending on υ_{e}, at $T_{\mathrm{MZI\text{-}D1}} > 0.5$ ($T_{\mathrm{MZI\text{-}D2}} < 0.5$). For example, with negligible dephasing in the MZI, that is, $\upsilon_{\mathrm{e}} = 1$, the anyonic visibility has a maximum at $T_{\mathrm{MZI\text{-}D1}} = 0.83$ and $T_{\mathrm{MZI\text{-}D2}} = 0.17$. Note that the AB oscillation amplitude is similar in both drains; however, the visibility (according to its definition) is $\upsilon_{e/3} \approx 20\%$ at D1 and $\upsilon_{e/3} \approx 100\%$ at D2 (Fig. 4a). Moreover, with decreased υ_{e}, the disparity between D1 and D2 becomes less evident. Illustrative examples of the interference patterns in both drains are shown in Fig. 4a.

We turn our attention to the experimentally observed visibility profiles in the small MZI. The interference pattern of the outer edge mode at filling $\boldsymbol{\nu} = 2$ is plotted in Fig. 4b. Multiple combinations of QPC transmissions $|t_{\mathrm{i}}|^2$ lead to the same average MZI transmission. We plot the measured visibility for multiple combinations of $|t_{\mathrm{i}}|^2$ (Fig. 4d). With a dephasing factor of $\eta = 0.91$ in $\boldsymbol{\nu} = 2$, the calculated visibility is plotted in Fig. 4f. The AB interference of the larger MZI, with $\eta = 0.67$, is shown in Supplementary Fig. 6.

The measured interference pattern of the outer $\boldsymbol{\nu} = 1/3$ mode is plotted in Fig. 4c, with the actual visibility $\upsilon_{e/3}$ plotted for many values of $|t_{\mathrm{i}}|^2$ as a function of $T_{\mathrm{MZI\text{-}D1}}$ (Fig. 4e) (assuring a measured partitioned charge of $e^* \approx e/3$). As shown in Fig. 4e (calculated values shown in Fig. 4g), the visibility peaks sharply at $\upsilon_{e/3} \approx 22.0\%$ (expected $\upsilon_{e/3}$ is ~15.6%) at an average transmission $T_{\mathrm{MZI\text{-}D1}}$ of ~0.6 (expected $T_{\mathrm{MZI\text{-}D1}}$ of ~ 0.76), indicating weak dephasing at the actual size of the MZI. The larger MZI behaved similarly with peak visibility of $\upsilon_{e/3} \approx 8.3\%$ at $T_{\mathrm{MZI\text{-}D1}} \approx 0.54$ (Table 1 and Supplementary Section 8).

The MZI is unique in the absence of any charging effects and thus exhibits pure quantum interference. In its fractional configuration, the interference is dressed, namely, a combined anyonic AB flux periodicity of h/e^* and fractional braiding phase of $2\pi e^*/e$, giving rise (as theoretically predicted) to a long waited flux periodicity of $\phi_0 = h/e$. Theory predicts a more complex interference in other exotic anyonic (that is, non-Abelian) states. The road is paved now for experimental tests of these predictions, which can unveil the topological order in these states.

Online content

Any methods, additional references, Nature Portfolio reporting summaries, source data, extended data, supplementary information, acknowledgements, peer review information; details of author contributions and competing interests; and statements of data and code availability are available at https://doi.org/10.1038/s41567-022-01899-z.

References

1. Halperin, B. I. Quantized Hall conductance, current-carrying edge states, and the existence of extended states in a two-dimensional disordered potential. *Phys. Rev. B* **25**, 2185–2190 (1982).
2. Wen, X.-G. in *Quantum Field Theory of Many-Body Systems: From the Origin of Sound to an Origin of Light and Electrons* (Oxford Univ. Press, 2004).

3. Kane, C. L. & Fisher, M. P. A. in *Perspectives in Quantum Hall Effects: Novel Quantum Liquids in Low-Dimensional Semiconductor Structures* (eds Das Sarma, S. & Pinczuk, A.) (John Wiley, 1996).
4. Stern, A. Anyons and the quantum Hall effect—a pedagogical review. *Ann. Phys.* **323**, 204–249 (2008).
5. Zheng, H. Z., Wei, H. P., Tsui, D. C. & Weimann, G. Gate-controlled transport in narrow GaAs/$Al_xGa_{1-x}As$ heterostructures. *Phys. Rev. B* **34**, 5635–5638 (1986).
6. Heiblum, M. & Feldman, D. E. Edge probes of topological order. *Int. J. Mod. Phys. A* **35**, 18 (2020).
7. Chang, A. M. Chiral Luttinger liquids at the fractional quantum Hall edge. *Rev. Mod. Phys.* **75**, 1449–1505 (2003).
8. Arovas, D., Schrieffer, J. R. & Wilczek, F. Fractional statistics and the quantum Hall effect. *Phys. Rev. Lett.* **53**, 722–723 (1984).
9. dePicciotto, R. et al. Direct observation of a fractional charge. *Nature* **389**, 162–164 (1997).
10. Saminadayar, L., Glattli, D. C., Jin, Y. & Etienne, B. Observation of the *e*/3 fractionally charged Laughlin quasiparticle. *Phys. Rev. Lett.* **79**, 2526–2529 (1997).
11. Leinaas, J. M. & Myrheim, J. On the theory of identical particles. *Nuovo Cim. B* **37**, 1–23 (1977).
12. Wilczek, F. Magnetic flux, angular momentum, and statistics. *Phys. Rev. Lett.* **48**, 1144–1146 (1982).
13. Halperin, B. I. Statistics of quasiparticles and the hierarchy of fractional quantized Hall states. *Phys. Rev. Lett.* **52**, 1583–1586 (1984).
14. Laughlin, R. B. Anomalous quantum Hall effect: an incompressible quantum fluid with fractionally charged excitations. *Phys. Rev. Lett.* **50**, 1395–1398 (1983).
15. Schuster, R. et al. Phase measurement in a quantum dot via a double-slit interference experiment. *Nature* **385**, 417–420 (1997).
16. Ofek, N. et al. Role of interactions in an electronic Fabry–Perot interferometer operating in the quantum Hall effect regime. *Proc. Natl Acad. Sci. USA* **107**, 5276–5281 (2010).
17. Zhang, Y. M. et al. Distinct signatures for Coulomb blockade and Aharonov-Bohm interference in electronic Fabry-Perot interferometers. *Phys. Rev. B* **79**, 241304 (2009).
18. Chamon, C. D. C., Freed, D. E., Kivelson, S. A., Sondhi, S. L. & Wen, X. G. Two point-contact interferometer for quantum Hall systems. *Phys. Rev. B* **55**, 2331–2343 (1997).
19. McClure, D. T., Chang, W., Marcus, C. M., Pfeiffer, L. N. & West, K. W. Fabry-Perot interferometry with fractional charges. *Phys. Rev. Lett.* **108**, 256804 (2012).
20. Choi, H. K. et al. Robust electron pairing in the integer quantum Hall effect regime. *Nat. Commun.* **6**, 7435 (2015).
21. Nakamura, J. et al. Aharonov–Bohm interference of fractional quantum Hall edge modes. *Nat. Phys.* **15**, 563–569 (2019).
22. Nakamura, J., Liang, S., Gardner, G. C. & Manfra, M. J. Direct observation of anyonic braiding statistics. *Nat. Phys.* **16**, 931–936 (2020).
23. Sivan, I. et al. Observation of interaction-induced modulations of a quantum Hall liquid's area. *Nat. Commun.* **7**, 12184 (2016).
24. Rosenow, B. & Simon, S. H. Telegraph noise and the Fabry-Perot quantum Hall interferometer. *Phys. Rev. B* **85**, 201302 (2012).
25. Ji, Y. et al. An electronic Mach–Zehnder interferometer. *Nature* **422**, 415–418 (2003).
26. Neder, I., Heiblum, M., Levinson, Y., Mahalu, D. & Umansky, V. Unexpected behavior in a two-path electron interferometer. *Phys. Rev. Lett.* **96**, 016804 (2006).
27. Neder, I. et al. Interference between two indistinguishable electrons from independent sources. *Nature* **448**, 333–337 (2007).
28. Neder, I., Heiblum, M., Mahalu, D. & Umansky, V. Entanglement, dephasing, and phase recovery via cross-correlation measurements of electrons. *Phys. Rev. Lett.* **98**, 036803 (2007).
29. Roulleau, P. et al. Finite bias visibility of the electronic Mach-Zehnder interferometer. *Phys. Rev. B* **76**, 161309 (2007).
30. Law, K. T., Feldman, D. E. & Gefen, Y. Electronic Mach-Zehnder interferometer as a tool to probe fractional statistics. *Phys. Rev. B* **74**, 045319 (2006).
31. Feldman, D. E. & Kitaev, A. Detecting non-Abelian statistics with an electronic Mach-Zehnder interferometer. *Phys. Rev. Lett.* **97**, 186803 (2006).
32. Roulleau, P. et al. Noise dephasing in edge states of the integer quantum Hall regime. *Phys. Rev. Lett.* **101**, 186803 (2008).
33. Roulleau, P. et al. Direct measurement of the coherence length of edge states in the integer quantum Hall regime. *Phys. Rev. Lett.* **100**, 126802 (2008).
34. Halperin, B. I., Stern, A., Neder, I. & Rosenow, B. Theory of the Fabry-Pérot quantum Hall interferometer. *Phys. Rev. B* **83**, 155440 (2011).
35. Rosenow, B. & Halperin, B. I. Influence of interactions on flux and back-gate period of quantum Hall interferometers. *Phys. Rev. Lett.* **98**, 106801 (2007).
36. Bhattacharyya, R., Banerjee, M., Heiblum, M., Mahalu, D. & Umansky, V. Melting of interference in the fractional quantum Hall effect: appearance of neutral modes. *Phys. Rev. Lett.* **122**, 246801 (2019).
37. Gurman, I., Sabo, R., Heiblum, M., Umansky, V. & Mahalu, D. Dephasing of an electronic two-path interferometer. *Phys. Rev. B* **93**, 121412 (2016).
38. Goldstein, M. & Gefen, Y. Suppression of interference in quantum Hall Mach-Zehnder geometry by upstream neutral modes. *Phys. Rev. Lett.* **117**, 276804 (2016).
39. Inoue, H. et al. Proliferation of neutral modes in fractional quantum Hall states. *Nat. Commun.* **5**, 4067 (2014).
40. Biswas, S. et al. Shot noise does not always provide the quasiparticle charge. *Nat. Phys.* **18**, 1476–1481 (2022).
41. Khanna, U., Goldstein, M. & Gefen, Y. Fractional edge reconstruction in integer quantum Hall phases. *Phys. Rev. B* **103**, L121302 (2021).
42. Khanna, U., Goldstein, M. & Gefen, Y. Emergence of neutral modes in Laughlin-like fractional quantum Hall phases. *Phys. Rev. Lett.* **129**, 146801 (2022).
43. Ponomarenko, V. V. & Averin, D. V. Mach-Zehnder interferometer in the fractional quantum Hall regime. *Phys. Rev. Lett.* **99**, 066803 (2007).
44. Feldman, D. E., Gefen, Y., Kitaev, A., Law, K. T. & Stern, A. Shot noise in an anyonic Mach-Zehnder interferometer. *Phys. Rev. B* **76**, 085333 (2007).
45. Campagnano, G. et al. Hanbury Brown-Twiss interference of anyons. *Phys. Rev. Lett.* **109**, 106802 (2012).
46. Kane, C. L. Telegraph noise and fractional statistics in the quantum Hall effect. *Phys. Rev. Lett.* **90**, 226802 (2003).
47. Thouless, D. & Gefen, Y. Fractional quantum Hall effect and multiple Aharonov-Bohm periods. *Phys. Rev. Lett.* **66**, 806–809 (1991).
48. Guyon, R., Devillard, P., Martin, T. & Safi, I. Klein factors in multiple fractional quantum Hall edge tunneling. *Phys. Rev. B* **65**, 153304 (2002).
49. Safi, I., Devillard, P. & Martin, T. Partition noise and statistics in the fractional quantum Hall effect. *Phys. Rev. Lett.* **86**, 4628–4631 (2001).
50. Ofek, N. *Interference Measurements at the Integer and Fractional Quantum Hall Effect*. PhD thesis, Weizmann Institute of Science (2010).

Data availability

Source data are provided with this paper. All other data related to this paper are available from the corresponding author upon reasonable request.

Acknowledgements

We acknowledge M. Banerjee, A. Das, D. E. Feldman, Y. Gefen, I. Neder and A. Stern for useful discussions, and the continuous support of the Sub-Micron Center staff. M.H. acknowledges support from the European Research Council under the European Community's Seventh Framework Program (FP7/2007-2013)/ERC under grant agreement no. 713351 and the Minerva foundation under grant no. 713534.

Author contributions

H.K.K. and S.B. designed and fabricated the devices. H.K.K. and S.B. performed the measurements and analysed the data with N.O. M.H. supervised the experiment and analysis. V.U. developed and grew the heterostructure supporting the two-dimensional electron gas. All the authors contributed to writing the manuscript.

Competing interests

The authors declare no competing interests.

Additional information

Supplementary information The online version contains supplementary material available at https://doi.org/10.1038/s41567-022-01899-z.

Correspondence and requests for materials should be addressed to Moty Heiblum.

Peer review information *Nature Physics* thanks the anonymous reviewers for their contribution to the peer review of this work.